

CONTENTS

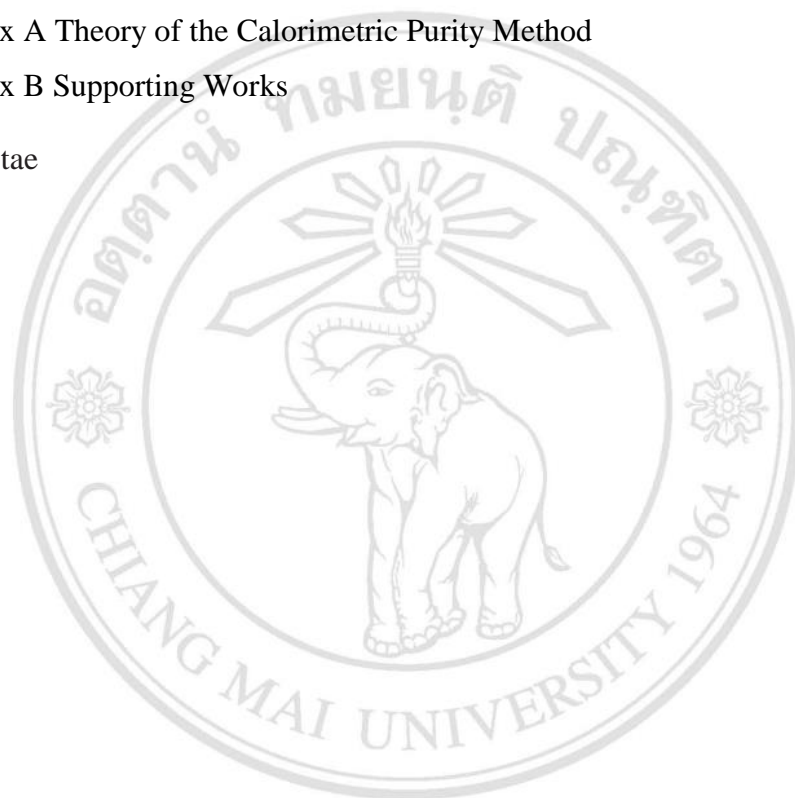
	Page
Acknowledgement	c
Abstract in Thai	d
Abstract in English	g
List of Tables	o
List of Figures	q
List of Abbreviations	y
List of Symbols	z
Statement of Originality in Thai	bb
Statement of Originality in English	cc
Chapter 1 Introduction	
1.1 Biodegradable Polymers	1
1.2 Physical and Biodegradable Properties of Aliphatic Polyesters for Use in Biomedical Applications	2
1.3 Absorbable Surgical Sutures	3
1.4 Historical Development of Synthetic Absorbable Sutures	4
1.5 Polyesters Synthesis	5
1.5.1 Mechanisms of ROP of Cyclic Esters	6
1.5.1.1 Cationic Ring-opening Polymerisation	7
1.5.1.2 Anionic Ring-opening Polymerisation	8
1.5.1.3 Coordination-Insertion Ring-opening Polymerisation	8
1.5.2 Organometallic compounds as Initiators for the ROP of Lactones and Lactides	9
1.5.2.1 Tin(II) 2-ethylhexanoate	10

1.5.2.2 Tin(II) Alkoxides	13
1.6 Kinetics of Ring-opening Polymerisation	13
1.7 Factors Governing the Ring-opening Polymerisability	14
1.7.1 Chemical Structure within the Ring	14
1.7.2 Ring Strain	15
1.7.3 Nature of Substituents External to the Ring	18
1.7.4 Nature of the Reaction Conditions Employed	19
1.8 Previous Work Relevant to This Study	20
1.9 Aim of This Study	27
Chapter 2 Materials and Instrumental Methods	
2.1 Chemicals, Apparatus and Instruments	30
2.1.1 Chemicals	30
2.1.2 Apparatus and Instruments	31
2.2 Monomer Purification	31
2.2.1 Purification and Purity Analysis of L-Lactide	31
2.2.2 Purification of ϵ -Caprolactone	33
2.3 Instrumental Methods	34
2.3.1 Fourier-Transform Infrared Spectroscopy (FT-IR)	34
2.3.2 Nuclear Magnetic Resonance Spectroscopy (NMR)	36
2.3.3 Thermal Analysis	38
2.3.3.1 Differential Scanning Calorimetry (DSC)	38
2.3.3.2 Thermogravimetry Analysis (TGA)	41
2.3.4 Molecular Weight Determination	44
2.3.4.1 Gel Permeation Chromatography (GPC)	44
2.3.4.2 Dilute-Solution Viscometry	45
2.3.5 Kinetic Determination by Dilatometry	47
2.4 Fabrication of PLC Fibre	48
2.4.1 Melt Spinning	48
2.4.2 Hot-drawing	50
2.4.3 Annealing	51
2.5 Tensile Testing	53

Chapter 3 Synthesis and Characterisation of Tin(II) alkoxides	
3.1 Purification of Reagents	58
3.1.1 Tin(II) Chloride	58
3.1.2 Tin(II) Octoate	58
3.1.3 Diols	58
3.1.4 Triethylamine	59
3.2 Synthesis and Characterisation of Tin(II) Alkoxides	60
3.2.1 Method 1	60
3.2.2 Method 2	68
Chapter 4 Kinetic studies by Dilatometry	
4.1 Homopolymer Polymerisation	76
4.1.1 Monomer	76
4.1.2 Initiators	77
4.2 Design of Kinetic Experiments	77
4.3 Limitation of Dilatometry	79
4.4 Dilatometric Data Analysis	80
4.4.1 Initial Meniscus Height	83
4.4.2 Kinetic Analysis	83
4.4.2.1 First-Order Kinetics Analysis	83
4.4.2.2 Zero-Order Kinetics Analysis	87
4.4.3 Preliminary Experiment Results	88
4.4.4 Dilatometry Results	94
Chapter 5 Synthesis and Characterisation of Polycaprolactone	
5.1 Synthesis and Purification of Poly(ϵ -caprolactone), PCL	118
5.2 Chemical Structure Analysis	121
5.2.1 Fourier Transform Infrared Spectroscopy (FT-IR)	121
5.2.2 Proton Nuclear Magnetic Resonance Spectroscopy ($^1\text{H-NMR}$)	126
5.3 Thermal Analysis	128
5.3.1 Differential Scanning Calorimetry (DSC)	128

5.3.2 Thermogravimetry Analysis (TGA)	131
5.4 Molecular Weight Determination by Dilute-Solution Viscometry	133
Chapter 6 Synthesis and Characterisation of Copolymers of L-lactide and ϵ -Caprolactone	
6.1 Monomer Preparation and Purification	140
6.2 Synthesis of Poly(L-lactide-co- ϵ -caprolactone), PLC 75:25 mol %	141
6.3 Characterisation of PLC Copolymers	142
6.3.1 Fourier-Transform Infrared Spectroscopy (FT-IR)	142
6.3.2 Nuclear Magnetic Resonance (NMR) Spectroscopy	147
6.3.2.1 Proton Nuclear Magnetic Resonance (^1H -NMR) Spectroscopy	147
6.3.2.2 Carbon-13 Nuclear Magnetic Resonance (^{13}C -NMR) Spectroscopy	151
6.3.3 Molecular Weight Determination	156
6.3.3.1 Gel Permeation Chromatography (GPC)	156
6.3.3.2 Dilute-Solution Viscometry	157
6.3.4 Thermal Analysis	162
6.3.4.1 Differential Scanning Calorimetry (DSC)	162
6.3.4.2 Thermogravimetry Analysis (TGA)	166
Chapter 7 Processing, Tensile Testing and Thermal Properties of PLC Monofilament Fibres	
7.1 Introduction	169
7.2 Melt Spinning	169
7.3 Tensile Testing	177
7.4 Off-line Hot-drawing and Annealing	178
7.5 Thermal Analysis by Differential Scanning Calorimetry	180
Chapter 8 Conclusions	
8.1 Novel Initiator Synthesis	190
8.2 Kinetic Studies by Dilatometry	193
8.3 Initiator Efficiency	194

8.4 Poly (L-lactide-co- ϵ -caprolactone) Synthesis	195
8.5 Melt Spinning of PLC into Monofilament Fibres	196
Suggestions for further work	198
References	199
Appendices	
Appendix A Theory of the Calorimetric Purity Method	210
Appendix B Supporting Works	213
Curriculum Vitae	243



ลิขสิทธิ์มหาวิทยาลัยเชียงใหม่
Copyright© by Chiang Mai University
All rights reserved

LIST OF TABLES

	Page
Table 1.1 The chemical structures of some commercial synthetic absorbable sutures	4
Table 1.2 Heats of combustion of cycloalkanes	16
Table 1.3 Polymerisability of cyclic ester compounds	17
Table 2.1 Chemicals used in this research project	30
Table 2.2 Apparatus and instruments used in this research project	31
Table 2.3 Dilute-solution viscosity terms currently in use	46
Table 3.1 Physical appearances and percentage yields of the purified Sn(OROH) ₂ products	62
Table 3.2 FT-IR absorption band assignments for the solid tin(II) alkoxides	64
Table 3.3 FT-IR absorption band assignments for the liquid tin(II) alkoxides	69
Table 4.1 The molecular formulae of initiators used for kinetic studies by dilatometry	77
Table 4.2 Densities of ϵ -caprolactone monomer at various temperatures	93
Table 4.3 Dilatometry data of ϵ -caprolactone polymerisation at 130 °C using 0.1 mol % Sn(Oct) ₂ as initiator	95
Table 4.4 Dilatometry data of ϵ -caprolactone polymerisation at 130 °C using 0.1 mol % mixture initiator (Sn(Oct) ₂ / DEG) as initiator	99
Table 4.5 Dilatometry data of ϵ -caprolactone polymerisation at 130 °C using 0.1 mol % mixture initiator (Sn(Oct) ₂ / EG) as initiator	103
Table 4.6 Dilatometry data of ϵ -caprolactone polymerisation at 130 °C using 0.1 mol % [Sn(Oct)] ₂ DEG as initiator	107
Table 4.7 Dilatometry data of ϵ -caprolactone polymerisation at 130 °C using 0.1 mol % [Sn(Oct)] ₂ EG as initiator	112
Table 4.8 Summary of kinetic results for ϵ -caprolactone polymerisation using different liquid initiating systems at 130 °C	116

Table 5.1 Chemical structures of the tin(II) alkoxide initiators used for PCL synthesis	119
Table 5.2 Main vibrational assignments in the FT-IR spectrum of the commercial PCL	122
Table 5.3 Main vibrational assignments in the FT-IR spectra of the purified PCL products using 0.10 mol % the solid tin(II) alkoxides initiators	124
Table 5.4 Main vibrational assignments in the FT-IR spectra of the purified PCL products using 0.10 mol % the liquid tin(II) alkoxide initiators	125
Table 5.5 Chemical shifts and relative peak intensities of the ¹ H-NMR spectra of PCL	128
Table 5.6 DSC (2 nd run) data analysis for PCL synthesized using various types and concentrations of the tin(II) alkoxide initiators	131
Table 5.7 Intrinsic viscosities, [η], and viscosity-average molecular weights, \bar{M}_v , of PCL obtained from dilute-solution viscometry in chloroform at 30 °C	133
Table 6.1 The calculated copolymer PLC compositions from ¹ H-NMR spectra	152
Table 6.2 Molecular weights of PLC copolymers from GPC	157
Table 6.3 Intrinsic viscosities, [η], of PLC copolymers from dilute-solution viscometry	161
Table 6.4 DSC results of the PLC copolymers	166
Table 7.1 Processing conditions used for melt spinning of the PLC copolymers obtained using the solid tin(II) alkoxide initiators	174
Table 7.2 Processing conditions used for melt spinning of the PLC copolymers obtained using the liquid tin(II) alkoxide initiators	175
Table 7.3 Conditions used in the off-line hot-drawing of the PLC fibres and the resultant tensile properties	181
Table 7.4 Tensile test and DSC data for the PLC fibres at various stages of processing	187

LIST OF FIGURES

	Page
Figure 1.1 Physical forms of (a) braided multifilament and (b) monofilament sutures	3
Figure 1.2 Schematic representation of the ring-opening polymerisation of a cyclic ester ($R = (CH_2)_{0-3}$ and/or (CHR''))	6
Figure 1.3 The reaction pathway for the ring-opening polymerisation of a cyclic ester by cationic initiation.	7
Figure 1.4 The reaction pathway for the ring-opening polymerisation of a cyclic ester by anionic initiation. Ring-opening of monomer by 1) acyl-oxygen bond cleavage and 2) alkyl-oxygen bond cleavage	8
Figure 1.5 The proposed reaction pathway for the ring-opening polymerisation of a cyclic ester by the coordination-insertion mechanism	9
Figure 1.6 Reaction scheme for intermolecular and intramolecular transesterification reactions	10
Figure 1.7 The main ring-opening polymerisation mechanism proposals with Tin(II) 2-ethylhexanoate as catalyst, a) complexation of a monomer and alcohol prior to ROP b) formation of a tin-alkoxide before ROP of ϵ -caprolactone	12
Figure 1.8 The variations of cyclic ester monomer structure	15
Figure 1.9 Changes in side-group repulsions on the ROP	19
Figure 2.1 DSC thermogram of purified L-lactide showing its melting peak used for purity analysis.	32
Figure 2.2 Van't Hoff plot derived from the melting peak data in Figure 2.1	33
Figure 2.3 Fractional vacuum distillation apparatus used for the purification of ϵ -caprolactone	34
Figure 2.4 Major vibrational modes for a nonlinear group, CH_2	35
Figure 2.5 Correlation table for the infrared bands	36
Figure 2.6 Correlation between the shift of a proton and the shift of the carbon	37

Figure 2.7 Principle components and layout of a power-compensated DSC cell showing the sample (S) and reference (R) micro furnaces	39
Figure 2.8 DSC thermogram showing the various temperature transitions that can occur in a semi-crystalline polymer	40
Figure 2.9 The Perkin Elmer DSC7 Differential Scanning Calorimeter	41
Figure 2.10 Diagram showing the furnace and balance arrangement in the Perkin-Elmer TGA7	42
Figure 2.11 A typical non-isothermal TG thermogram for polymer showing the various reaction parameters derived from the curve	42
Figure 2.12 The Perkin Elmer TGA7 Thermogravimetric Analyzer	43
Figure 2.13 GPC-SEC separation mechanism	44
Figure 2.14 PL-GPC 50 Plus Gel Permeation Chromatography	45
Figure 2.15 Small-scale melt spinning apparatus	49
Figure 2.16 A schematic drawing of molecular orientation changes during the fibre formation at the extrusion	50
Figure 2.17 Schematic representation of molecular and crystal orientation in polymer fibre developed under drawing process	51
Figure 2.18 Schematic representation of crystallisation in polymer fibre developed under free annealing process	52
Figure 2.19 Schematic representation of both crystallization and orientation of crystallites along the fibre axis in polymer fibre developed under fixed annealing process	52
Figure 2.20 A typical stress-strain curve for semi-crystalline polymers	53
Figure 2.21 Typical stress-strain curves	55
Figure 2.22 Universal Mechanical Testing Machine used for fibre tensile testings	56
Figure 2.23 Photograph of the bollard grips	57
Figure 3.1 Simple distillation apparatus for purification of reagents	60
Figure 3.2 Apparatus used for the synthesis of the solid tin(II) alkoxides by Method 1	61
Figure 3.3 FT-IR spectra of the solid tin(II) alkoxides	64
Figure 3.4 NMR spectra of the solid tin(II) alkoxides	65
Figure 3.5 DSC Thermograms of the solid tin(II) alkoxides	66

Figure 3.6 TGA Thermograms for the solid tin(II) alkoxides	67
Figure 3.7 Apparatus used for the synthesis of the liquid tin(II) alkoxides by Method 2	68
Figure 3.8 FT-IR spectra of the liquid tin(II) alkoxides	69
Figure 3.9 Comparison of FT-IR spectra of $[\text{Sn}(\text{Oct})_2]$ DEG initiators synthesised from difference mole ratios of $\text{Sn}(\text{Oct})_2$: DEG	70
Figure 3.10 NMR spectrum of $[\text{Sn}(\text{Oct})_2]$ DEG	71
Figure 3.11 NMR spectrum of $[\text{Sn}(\text{Oct})_2]$ EG	72
Figure 3.12 LC-MS spectra of stannous octoate ($\text{Sn}(\text{Oct})_2$)	73
Figure 3.13 LC-MS spectra of diethylene glycol (DEG)	73
Figure 3.14 LC-MS spectra of octanoic acid (OctH)	74
Figure 3.15 LC-MS spectra of $[\text{Sn}(\text{Oct})_2]$ DEG	74
Figure 3.16 TGA thermograms of the liquid alkoxides	75
Figure 4.1 Dilatometry set-up used in kinetic studies of ROP of ϵ -CL	79
Figure 4.2 Dilatometric data for ϵ -caprolactone polymerisation at 130 °C using 0.10 mol % $\text{Sn}(\text{Oct})_2$; initial oil bath temperature set at (a) 130 °C and (b) 140 °C	89
Figure 4.3 Extrapolation of h to zero time (h_0 at $t = 0$) and at constant height (h_∞) for ϵ -caprolactone polymerisation using 0.1 mol % $\text{Sn}(\text{Oct})_2$ / EG as initiator at 130 °C	90
Figure 4.4 Kinetic profile of % conversion against time for ϵ -caprolactone using 0.1 mol % $\text{Sn}(\text{Oct})_2$ / EG as initiator at 130 °C	90
Figure 4.5 First-order rate plot from dilatometry for ϵ -caprolactone using 0.1 mol % $\text{Sn}(\text{Oct})_2$ / EG as initiator at 130 °C	91
Figure 4.6 Zero-order rate plot from dilatometry for ϵ -caprolactone using 0.1 mol % $\text{Sn}(\text{Oct})_2$ / EG as initiator at 130 °C	92
Figure 4.7 The linear decrease in density as a function of temperature for ϵ -caprolactone monomer	93
Figure 4.8 Extrapolation of h to zero time (h_0 at $t = 0$) for ϵ -caprolactone polymerisation using 0.1 mol % $\text{Sn}(\text{Oct})_2$ as initiator at 130 °C	97
Figure 4.9 Kinetic profile from dilatometry of % conversion against time for ϵ -caprolactone using 0.1 mol % $\text{Sn}(\text{Oct})_2$ as initiator at 130 °C	97

Figure 4.10 First-order rate plot from dilatometry for ϵ -caprolactone using 0.1 mol % $\text{Sn}(\text{Oct})_2$ as initiator at 130 °C	98
Figure 4.11 Zero-order rate plot from dilatometry for ϵ -caprolactone using 0.1 mol % $\text{Sn}(\text{Oct})_2$ as initiator at 130 °C	98
Figure 4.12 Extrapolation of h to zero time (h_0 at $t = 0$) for ϵ -caprolactone polymerisation using 0.1 mol % $\text{Sn}(\text{Oct})_2$ / DEG as initiator at 130 °C	101
Figure 4.13 Kinetic profile from dilatometry of % conversion against time for ϵ -caprolactone using 0.1 mol % $\text{Sn}(\text{Oct})_2$ / DEG as initiator at 130 °C	101
Figure 4.14 First-order rate plot from dilatometry for ϵ -caprolactone using 0.1 mol % $\text{Sn}(\text{Oct})_2$ / DEG as initiator at 130 °C	102
Figure 4.15 Zero-order rate plot from dilatometry for ϵ -caprolactone using 0.1 mol % $\text{Sn}(\text{Oct})_2$ / DEG as initiator at 130 °C	102
Figure 4.16 Extrapolation of h to zero time (h_0 at $t = 0$) and at constant height (h_∞) for ϵ -caprolactone polymerisation using 0.1 mol% $\text{Sn}(\text{Oct})_2/\text{EG}$ as initiator at 130 °C	105
Figure 4.17 Kinetic profile from dilatometry of % conversion against time for ϵ -caprolactone using 0.1 mol % $\text{Sn}(\text{Oct})_2$ / EG as initiator at 130 °C	105
Figure 4.18 First-order rate plot from dilatometry for ϵ -caprolactone using 0.1 mol % $\text{Sn}(\text{Oct})_2$ / EG as initiator at 130 °C	106
Figure 4.19 Zero-order rate plot from dilatometry for ϵ -caprolactone using 0.1 mol % $\text{Sn}(\text{Oct})_2$ / EG as initiator at 130 °C	106
Figure 4.20 Extrapolation of h to zero time (h_0 at $t = 0$) for ϵ -caprolactone polymerisation using 0.1 mol % $[\text{Sn}(\text{Oct})]_2$ DEG as initiator at 130 °C	110
Figure 4.21 Kinetic profile from dilatometry of % conversion against time for ϵ -caprolactone using 0.1 mol % $[\text{Sn}(\text{Oct})]_2$ DEG as initiator at 130 °C	110
Figure 4.22 First-order rate plot from dilatometry for ϵ -caprolactone using 0.1 mol % $[\text{Sn}(\text{Oct})]_2$ DEG as initiator at 130 °C	111
Figure 4.23 Zero-order rate plot from dilatometry for ϵ -caprolactone using 0.1 mol % $[\text{Sn}(\text{Oct})]_2$ DEG as initiator at 130 °C	111
Figure 4.24 Extrapolation of h to zero time (h_0 at $t = 0$) for ϵ -caprolactone polymerisation using 0.1 mol % $[\text{Sn}(\text{Oct})]_2\text{EG}$ as initiator at 130 °C	114

Figure 4.25 Kinetic profile from dilatometry of % conversion against time for ϵ -caprolactone using 0.1 mol % $[\text{Sn}(\text{Oct})]_2\text{EG}$ as initiator at 130 °C	114
Figure 4.26 First-order rate plot from dilatometry for ϵ -caprolactone using 0.1 mol % $[\text{Sn}(\text{Oct})]_2\text{EG}$ as initiator at 130 °C	115
Figure 4.27 Zero-order rate plot from dilatometry for ϵ -caprolactone using 0.1 mol % $[\text{Sn}(\text{Oct})]_2\text{EG}$ as initiator at 130 °C	115
Figure 5.1 Apparatus used in the ring-opening bulk polymerisation of ϵ -CL	120
Figure 5.2 Apparatus used for PCL purification by re-precipitation from solution	120
Figure 5.3 Infrared spectrum of commercial PCL	121
Figure 5.4 Infrared spectra of the purified PCL using the solid $\text{Sn}(\text{PEG}300)_2$ initiator	122
Figure 5.5 Infrared spectra of the purified PCL using the solid $\text{Sn}(\text{PPG}400)_2$ initiator	123
Figure 5.6 Infrared spectra of the purified PCL using the solid $\text{Sn}(\text{DEG})_2$ initiator	123
Figure 5.7 Infrared spectra of the purified PCL using the liquid $[\text{Sn}(\text{Oct})]_2\text{DEG}$ initiator	124
Figure 5.8 Infrared spectra of the purified PCL using the liquid $[\text{Sn}(\text{Oct})]_2\text{EG}$ initiator	125
Figure 5.9 $^1\text{H-NMR}$ spectrum of the commercial PCL	126
Figure 5.10 $^1\text{H-NMR}$ spectrum of PCL synthesised using 0.10 mol % of the solid $\text{Sn}(\text{DEG})_2$ initiator	127
Figure 5.11 $^1\text{H-NMR}$ spectrum of PCL synthesised using 0.10 mol % of the liquid $[\text{Sn}(\text{Oct})]_2\text{DEG}$ initiator	127
Figure 5.12 DSC (2 nd run) thermograms of PCL using 0.02 mol % of the various tin(II) alkoxides	129
Figure 5.13 DSC (2 nd run) thermograms of PCL using 0.10 mol % of the various tin(II) alkoxides	130
Figure 5.14 DSC (2 nd run) thermograms of PCL using 0.20 mol % of the various tin(II) alkoxides.	130
Figure 5.15 TGA thermograms of the purified PCL products synthesised using the various tin(II) alkoxide initiators at different concentrations: (a) 0.02 mol % (b) 0.10 mol % and (c) 0.20 mol % (Heating rate = 20 °C/min, N_2 atmosphere)	132
Figure 5.16 Plots of η_{red} and η_{inh} vs concentration of PCL synthesised using the solid initiator, $\text{Sn}(\text{PEG}300)_2$	134

Figure 5.17 Plots of η_{red} and η_{inh} vs concentration of PCL synthesised using the solid initiator, Sn(PPG400)_2	135
Figure 5.18 Plots of η_{red} and η_{inh} vs concentration of PCL synthesised using the solid initiator, Sn(DEG)_2	136
Figure 5.19 Plots of η_{red} and η_{inh} vs concentration of PCL synthesised using the liquid initiators, $[\text{Sn(Oct)}]_2\text{DEG}$	137
Figure 5.20 Plots of η_{red} and η_{inh} vs concentration of PCL synthesised using the liquid initiators, $[\text{Sn(Oct)}]_2\text{EG}$	138
Figure 6.1 Apparatus used for copolymerisation	141
Figure 6.2 FT-IR spectra of PLC using Sn(Oct)_2 as initiator	142
Figure 6.3 FT-IR spectra of PLC using mixed initiator ($\text{Sn(Oct)}_2 / \text{DEG}$)	143
Figure 6.4 FT-IR spectra of PLC using mixed initiator ($\text{Sn(Oct)}_2 / \text{EG}$)	143
Figure 6.5 FT-IR spectrum of PLC using solid Sn(PEG300)_2 as initiator	144
Figure 6.6 FT-IR spectrum of PLC using solid Sn(PPG400)_2 as initiator	144
Figure 6.7 FT-IR spectrum of PLC using solid Sn(PPG1200)_2 as initiator	145
Figure 6.8 FT-IR spectra of PLC using liquid $[\text{Sn(Oct)}]_2\text{DEG}$ (2.1:1) as initiator	145
Figure 6.9 FT-IR spectra of PLC using liquid $[\text{Sn(Oct)}]_2\text{DEG}$ (3.0:1) as initiator	146
Figure 6.10 FT-IR spectrum of PLC using liquid $[\text{Sn(Oct)}]_2\text{EG}$ as initiator	146
Figure 6.11 400 MHz $^1\text{H-NMR}$ spectra of the PLC copolymers using: the solid tin(II) alkoxide initiators	148
Figure 6.12 400 MHz $^1\text{H-NMR}$ spectra of the PLC copolymers using: the liquid tin(II) alkoxide initiators	149
Figure 6.13 $^1\text{H-NMR}$ spectrum of PLC using 0.02 mol % Sn(Oct)_2 initiator	150
Figure 6.14 Typical $^{13}\text{C-NMR}$ spectrum of a PLC copolymer	153
Figure 6.15 Expanded carbonyl regions of the $^{13}\text{C-NMR}$ spectra of the PLC copolymers using the various initiators: (a) 0.01 mol % Sn(Oct)_2 (b) 0.02 mol % Sn(Oct)_2 (c) 0.01 mol % $[\text{Sn(Oct)}]_2\text{DEG}$ (3:1) (d) 0.02 mol % $[\text{Sn(Oct)}]_2\text{DEG}$ (3:1) and (e) 0.02 mol % $[\text{Sn(Oct)}]_2\text{EG}$	155
Figure 6.16 Plots of η_{red} and η_{inh} vs concentration of PLC synthesised using Sn(Oct)_2 and mixed initiators	158

Figure 6.17 Plots of η_{red} and η_{inh} vs concentration of PLC synthesised using the solid initiators	159
Figure 6.18 Plots of η_{red} and η_{inh} vs concentration of PLC synthesised using the liquid initiators	160
Figure 6.19 DSC thermograms of the synthesised the PLC copolymers using $Sn(Oct)_2$ and the mixed initiators	163
Figure 6.20 DSC thermograms of the PLC copolymers using 0.01 and 0.02 mol % of the various solid tin(II) alkoxide initiators	164
Figure 6.21 DSC thermogram of the PLC copolymers using 0.01 mol % of the various the liquid tin(II) alkoxide initiators	165
Figure 6.22 TG thermograms of the PLC copolymers using $Sn(Oct)_2$ and the mixed initiators	167
Figure 6.23 TG thermograms of the PLC copolymers using the solid tin(II) alkoxide initiators	167
Figure 6.24 TG thermograms of the PLC copolymers using the liquid tin(II) alkoxide initiators	168
Figure 7.1 Small-scale melt spinning apparatus	170
Figure 7.2 The various melt spinning apparatus accessories used in the preparation of PLC rods	171
Figure 7.3 The assembled cylinder used for making a copolymer rod	171
Figure 7.4 The various accessories used in the melt spinning of the pre-forming PLC rods	172
Figure 7.5 The assembled cylinder used for fibre processing	173
Figure 7.6 (a) Extruded filament being cooled (quenched) by passing through the cooling bath and (b) being wound around the take-up rollers before being collected on a bobbin	173
Figure 7.7 Stress-strain curves of the PLC as-spun fibres using initiators	178
Figure 7.8 Stress-strain curves of the PLC fibres (0.02 mol % $Sn(PPG400)_2$ solid initiator) after 1 st hot-drawing at 40 and 45 °C	182
Figure 7.9 Stress-strain curves of the PLC fibres (0.01 mol % $[Sn(Oct)]_2$ DEG (2.1:1) liquid initiator) after 1 st hot-drawing at 40, 50 and 60 °C	182

Figure 7.10 Stress-strain curves of the PLC fibres (0.01 mol % [Sn(Oct)] ₂ DEG (3.0:1) liquid initiator) after 1 st hot-drawing at 50, 60 and 70 °C	183
Figure 7.11 Stress-strain curves of the PLC fibres (0.02 mol % [Sn(Oct)] ₂ DEG (3.0:1) liquid initiator) after 1 st hot-drawing at 40, 55 and 70 °C	183
Figure 7.12 Stress-strain curves of the PLC fibres at various stages of processing (0.01 mol % [Sn(Oct)] ₂ DEG (2.1:1) initiator)	184
Figure 7.13 Stress-strain curve of the PLC fibres at various stages of processing (0.01 mol % [Sn(Oct)] ₂ DEG (3.0:1) initiator)	184
Figure 7.14 Stress-strain curves of the PLC fibres at various stages of processing (0.02 mol % [Sn(Oct)] ₂ DEG (3.0:1) initiator)	185
Figure 7.15 DSC thermograms of the PLC fibres at various stages of processing (0.01 mol % [Sn(Oct)] ₂ DEG (2.1:1) initiator)	185
Figure 7.16 DSC thermograms of the PLC fibres at various stages of processing (0.01 mol % [Sn(Oct)] ₂ DEG (3.0:1) initiator)	186
Figure 7.17 DSC thermograms of the PLC fibres at various stages of processing (0.02 mol % [Sn(Oct)] ₂ DEG (3.0:1) initiator)	186

LIST OF ABBREVIATIONS

CL	ϵ -caprolactone
PCL	poly(ϵ -caprolactone)
PLC	poly(L-lactide- <i>co</i> - ϵ -caprolactone)
ROP	Ring-opening polymerization
Sn(OR) ₂	Tin(II) alkoxides
CDCl ₃	Deuterated chloroform
DMSO	Dimethyl sulfoxide
THF	Tetrahydrofuran
FT-IR	Fourier-transform infrared spectroscopy
NMR	Nuclear magnetic resonance
DSC	Differential scanning calorimetry
TGA	Thermogravimetric analysis
GPC	Gel permeation chromatography
PD	Polydispersity

LIST OF SYMBOLS

\bar{M}_n	Number-average molecular weight
\bar{M}_w	Weight-average molecular weight
\bar{M}_v	Viscosity-average molecular weight
T_c	Crystallisation temperature
T_m	Melting temperature
T_d	Decomposition temperature
ΔG_p	Free energy change for polymerization
ΔG_p°	Standard state free energy change for polymerisation
ΔH_p	Enthalpy change for polymerisation
ΔS_p	Entropy change for polymerisation
ΔS_m	Entropy of melting
ΔH_m	Heat (enthalpy) of melting
ΔH_m^*	Heat of melting of a 100 % crystalline polymer
$[\eta]$	Intrinsic viscosity
R_p	Rate of polymerization

k_{app}	Apparent rate constant
k_p	Rate constant of propagation (polymerisation)
k_1	First-order rate constant
k_0	Zero-order rate constant\
$\text{mol l}^{-1} \text{min}^{-1}$	mol per litre per minute



ลิขสิทธิ์มหาวิทยาลัยเชียงใหม่
 Copyright© by Chiang Mai University
 All rights reserved

ข้อความแห่งการริเริ่ม

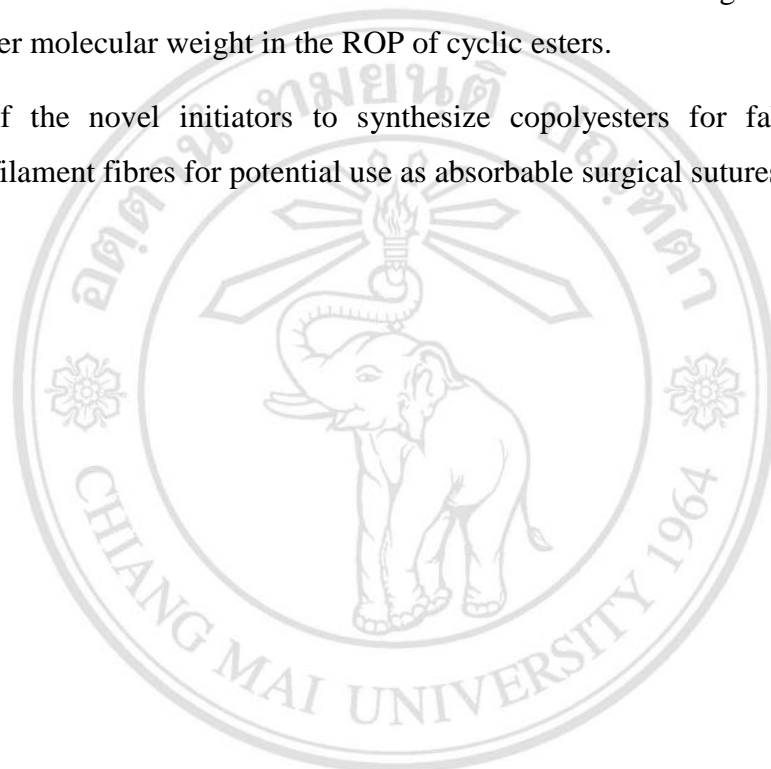
- 1) การสังเคราะห์ตัวริเริ่มปฏิกิริยาชนิดใหม่ เพื่อใช้สำหรับพอลิเมอร์ไรเซชันแบบเปิดวงของไซคลิกเอสเทอร์
- 2) การศึกษาประสิทธิภาพของตัวริเริ่มปฏิกิริยาชนิดใหม่ เพื่อใช้ในการควบคุมจลนศาสตร์ และน้ำหนักโมเลกุลของพอลิเมอร์ ในการเกิดปฏิกิริยาการเปิดวงของไซคลิกเอสเทอร์
- 3) การใช้ตัวริเริ่มปฏิกิริยาชนิดใหม่เพื่อสังเคราะห์โพลีเอสเทอร์ สำหรับผลิตเป็นเส้นใยเดี่ยว เพื่อใช้เป็นไหมละลายที่มีประสิทธิภาพในงานศัลยกรรม



ลิขสิทธิ์มหาวิทยาลัยเชียงใหม่
Copyright© by Chiang Mai University
All rights reserved

STATEMENT OF ORIGINALITY

1. Synthesis of novel initiators for use in the ring-opening polymerisation (ROP) of cyclic esters.
2. Studies of the efficiencies of the novel initiators in controlling the kinetics and polymer molecular weight in the ROP of cyclic esters.
3. Use of the novel initiators to synthesize copolyesters for fabricating into monofilament fibres for potential use as absorbable surgical sutures.



ลิขสิทธิ์มหาวิทยาลัยเชียงใหม่
Copyright© by Chiang Mai University
All rights reserved